Supplement of Solid Earth, 11, 173–184, 2020
https://doi.org/10.5194/se-11-173-2020-supplement

Solid Earth Open Access EGU

Supplement of

Observation and explanation of spurious seismic signals emerging in teleseismic noise correlations

Lei Li et al.

Correspondence to: Lei Li (lilei@ies.ac.cn)

Computation of correlation function

Figure S1 describes the computation of the correlation function between two time series. The diagram is self-explained.

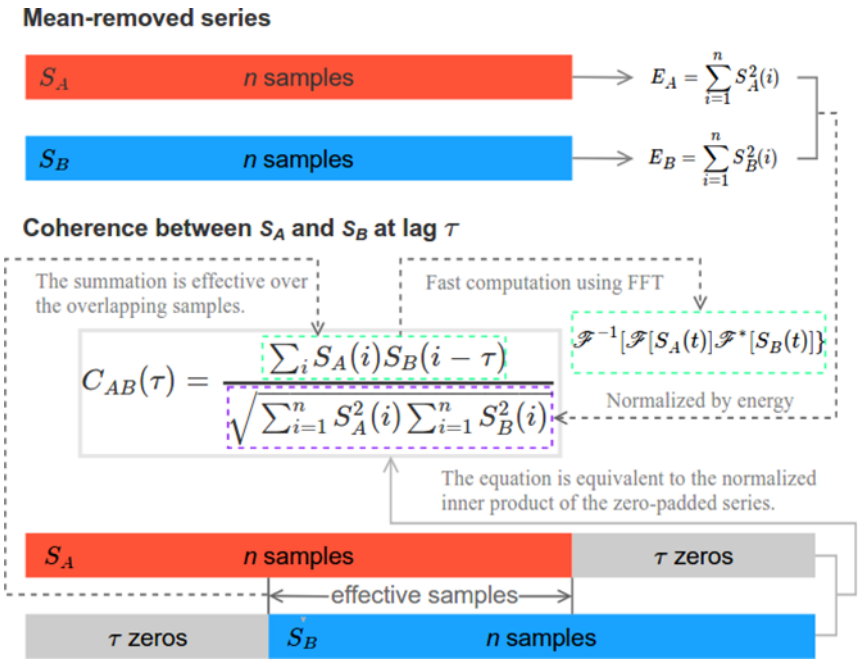

Figure S1: Schematic for the computation of the correlation function between two mean-removed time series.

Broadband double-array correlations

Figure S2 shows the FNET-LAPNET correlations in the period band of 1 s to 100 s. The spurious phase is clearly visible in the acausal section. The beamed waveform of the acausal spurious phase and its frequency spectrum are plotted in Fig. S3. It has a peak period of 6.2 s.

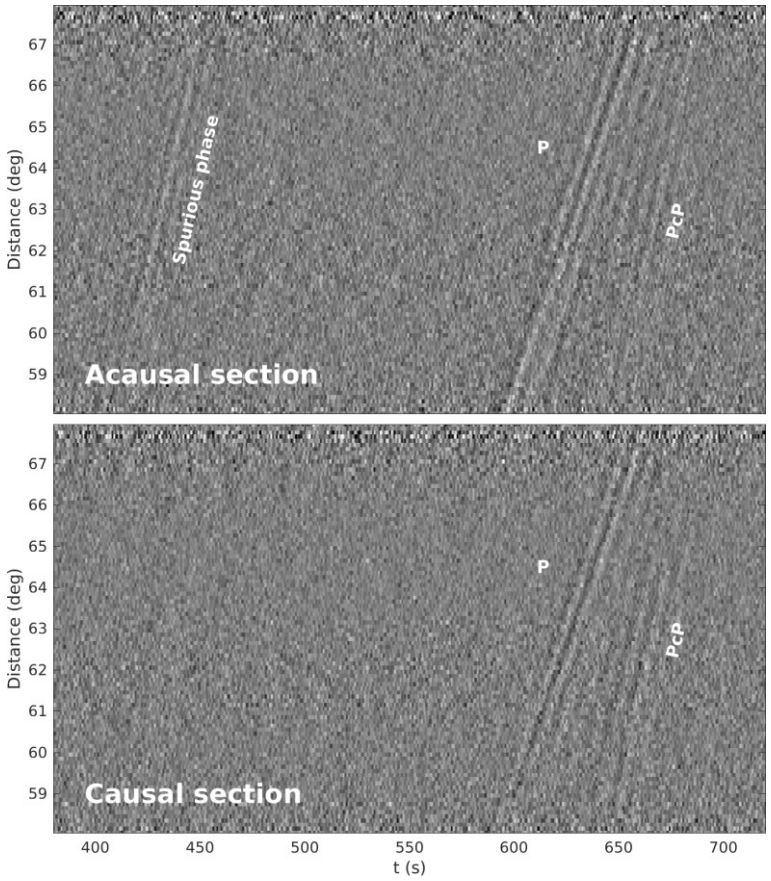

Figure S2: Broadband (1 to 100 s) sections of the acausal and causal parts of the vertical-vertical noise correlations stacked in 0.1° distance bins.

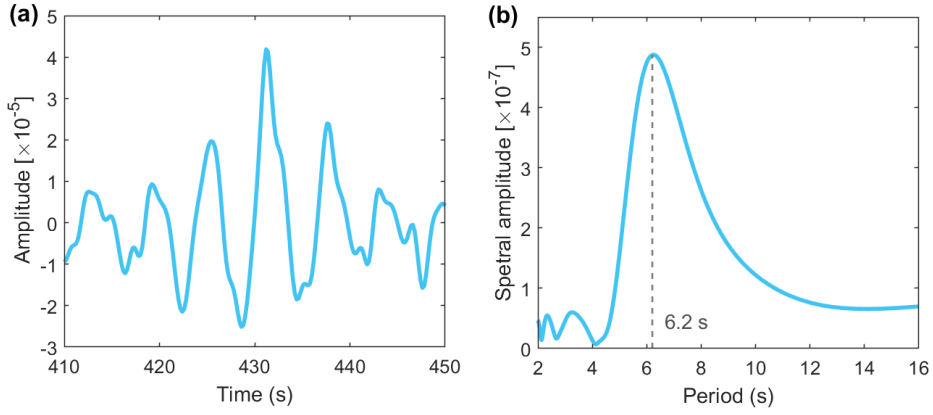

Figure S3: (a) Beamed waveform and (b) amplitude spectrum of the spurious phase in the broadband of 1 to 100 s.

Stationary-phase examples

Figure S4 shows the double-array slowness analysis for the noise-derived acausal P wave and the synthetic experiment for the generation of the inter-receiver P wave from P-PP correlations that can be explained by the traditional stationary-phase arguments, in contrast to the results of slowness analysis for the acausal spurious phase in Fig. 5 and the quasi-stationary-phase explanation in Fig. 9. Slowness analysis in Fig. S4a indicates the correlated waves responsible for the inter-receiver P wave have almost identical slowness. The schematic in Fig. S4b shows that the P wave emanating from the stationary location (label A) to the first receiver and the PP wave to the second receiver have a common slowness and a common P path. The correlation operator cancels the common path and accordingly extracts the phase delay between two receivers. Fig. S4c shows the synthetic source averaging experiment for P-PP correlations. The stationary location corresponds to the extreme point on the dashed time-delay curve. Amplitudes in the P-PP correlations for sources outside the shaded stationary-phase region cancel out by the averaging. The time delay at the maximum of the envelope of the stacked waveform matches exactly with the theoretical travel time of the inter-receiver P wave.

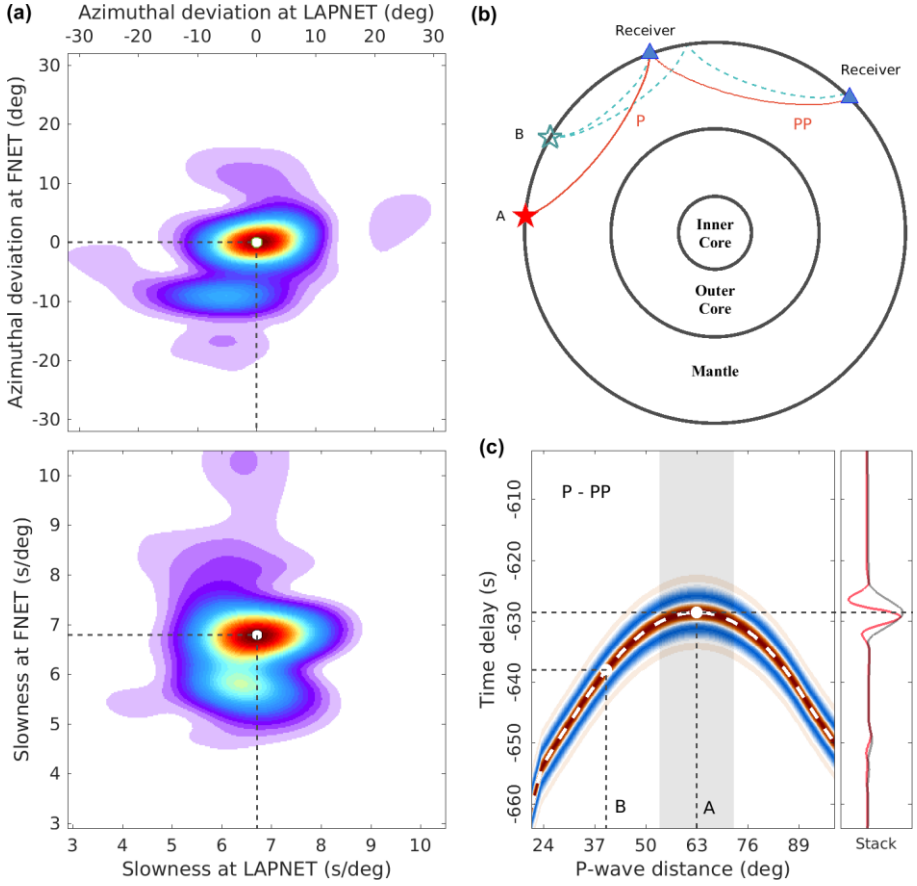

Figure S4: (a) Results of double-array slowness analysis for the acausal P wave. (b) Ray paths of the correlated P and PP waves from distributed sources. Source A is placed at the stationary location. Label B denotes any noise source on the global surface outside the stationary-phase region. For simplicity, the correlations between higher-order multiples like PP-PPP that can also give rise to P waves are neglected. (c) Reconstruction of the inter-receiver P wave from the P-PP correlations by source averaging, explained by the traditional stationary-phase theory.

In the global section of coda correlations by Phạm et al. (2018), there is also a spurious signal at ~430 s time delay and 63° separation distance (see their fig. 2). Phạm et al. (2018) ascribed the signal to the correlation between cS and cPPcP phases for sources distributed on the core-mantle boundary (phase naming in their customized conventions; equivalent to s and pPcP phases in IASPEI convention). Here we consider the PcS-PcPPcP correlation, which is an equivalence to their cS-cPPcP correlation but for sources on the global surface. Figure S5 depicts the stationary-phase arguments for the PcS-PcPPcP correlation. However, similar to the discussion about the PcP-PKPab correlation in the main text, the correlated waves are too weak in the ballistic wavefield to be responsible for the spurious phase observed in this study (cf. Fig. 7 in main text). And another strong argument is that, the slownesses of PcS and PcPPcP are quite distinct from the slowness estimates in Fig. 2a.

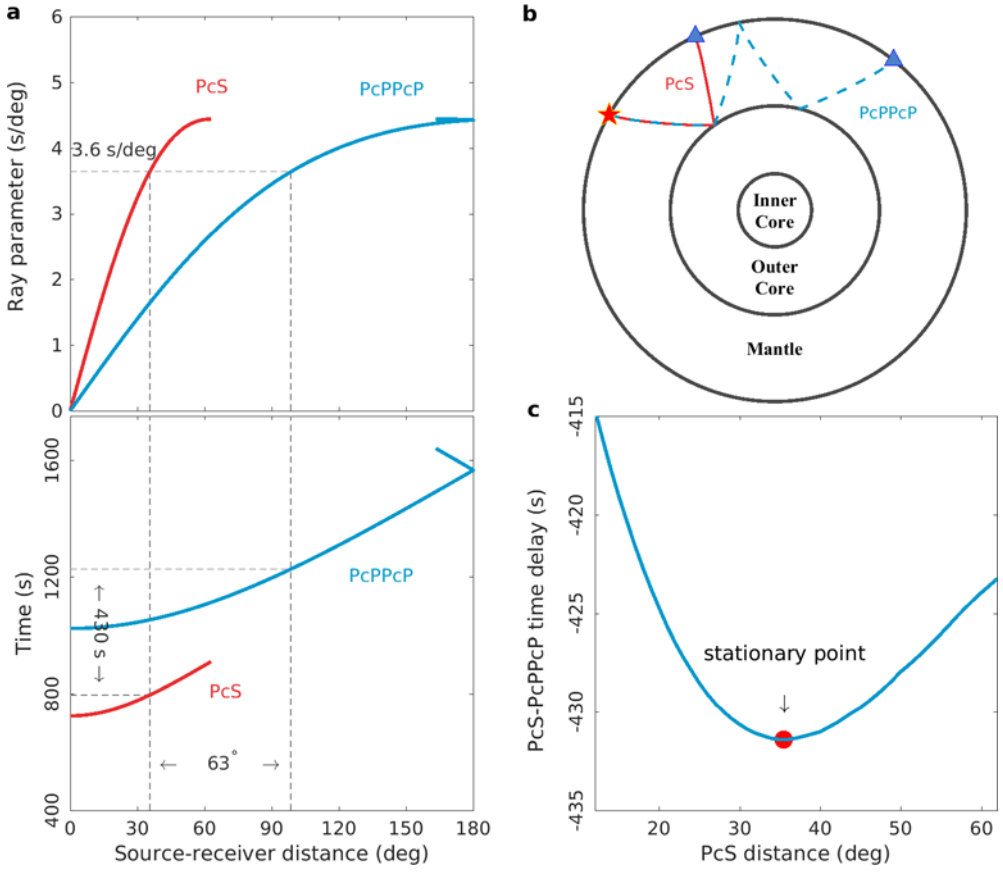

Figure S5: (a) Theoretical curves of ray parameters and travel times of PcS and PcPPcP. (b) Ray paths of PcS and PcPPcP from source at stationary location. (c) PcS-PcPPcP time delays for distributed sources.

Numerical simulations of P-PKPab correlations

Figure S6 shows the synthetic P-PKPab correlations for the planar model with sources along the great circle (one-dimensional source distribution) and the spherical model with sources over the global surface (two-dimensional source distribution), using the wave-based method described in section 6 of main text. The synthetic correlations are filtered between 5 s and 10 s periods. The spurious phase is visible in a broader distance range in Fig. S6a than in Fig.S6b. The time-distance curves are picked from the maximum on the envelope of each trace. In the common distance range, the two time-distance curves agree well with each other.

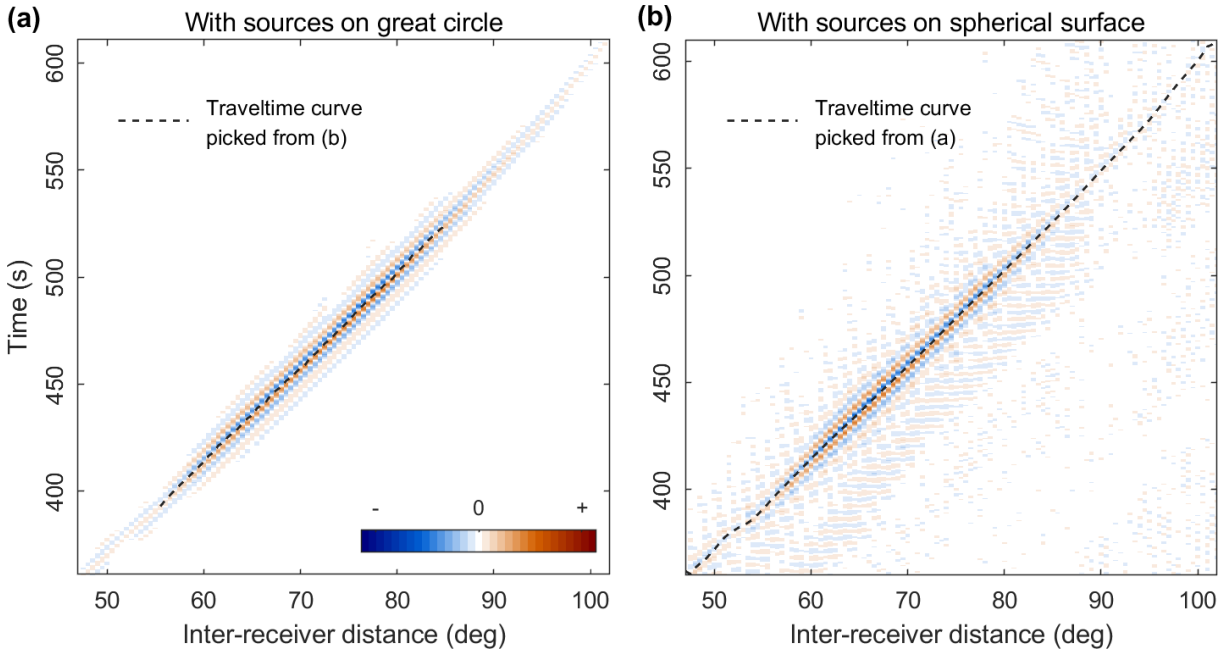

Figure S6: Wave-based simulations of P-PKPab correlations with sources (a) on the great circle and (b) on the global surface.